Absolute Dimensions of the Metallic-line Eclipsing Binary V501 Monocerotis

Torres, G.; Lacy, C. H. S.; Pavlovski, Krešimir; Fekel, F.C.; Muterspaugh, M.W.

Source / Izvornik: **Astronomical Journal, 2015, 150**

Journal article, Published version
Rad u časopisu, Objavljena verzija rada (izdavačev PDF)

https://doi.org/10.1088/0004-6256/150/5/154

Permanent link / Trajna poveznica: https://urn.nsk.hr/urn:nbn:hr:217:921431

Rights / Prava: In copyright / Zaštićeno autorskim pravom.

Download date / Datum preuzimanja: **2024-12-24**

Repository / Repozitorij:

Repository of the Faculty of Science - University of Zagreb

The Astronomical Journal, 150:154 (11pp), 2015 November doi:10.1088/0004-6256/150/5/154
© 2015. The American Astronomical Society. All rights reserved.

ABSOLUTE DIMENSIONS OF THE METALLIC-LINE ECLIPSING BINARY V501 MONOCEROTIS

Guillermo Torres[1], Claud H. Sandberg Lacy[2], Krešimir Pavlovski[3], Francis C. Fekel[4], and Matthew W. Muterspaugh[4,5]
[1] Harvard-Smithsonian Center for Astrophysics, 60 Garden St., Cambridge, MA 02138, USA; gtorres@cfa.harvard.edu
[2] Department of Physics, University of Arkansas, Fayetteville, AR 72701, USA
[3] Department of Physics, Faculty of Science, University of Zagreb, Bijenička cesta 32, 10000 Zagreb, Croatia
[4] Center of Excellence in Information Systems, Tennessee State University, Nashville, TN 37209, USA
[5] Department of Mathematical Sciences, College of Science and Mathematics, Tennessee State University, Boswell Science Hall, Nashville, TN 37209, USA
Received 2015 August 21; accepted 2015 September 24; published 2015 October 21

ABSTRACT

We report extensive high-resolution spectroscopic observations and *V*-band differential photometry of the slightly eccentric 7.02 day detached eclipsing binary V501 Mon (A6m+F0), which we use to determine its absolute dimensions to high precision (0.3% for the masses and 1.8% for the radii, or better). The absolute masses, radii, and temperatures are $M_{\rm A} = 1.6455 \pm 0.0043\,M_{\odot}$, $R_{\rm A} = 1.888 \pm 0.029\,R_{\odot}$, and $T_{\rm eff}^{\rm A} = 7510 \pm 100$ K for the primary and $M_{\rm B} = 1.4588 \pm 0.0025\,M_{\odot}$, $R_{\rm B} = 1.592 \pm 0.028\,R_{\odot}$, and $T_{\rm eff}^{\rm B} = 7000 \pm 90$ K for the secondary. Apsidal motion has been detected, to which General Relativity contributes approximately 70%. The primary star is found to be a metallic-line A star. A detailed chemical analysis of the disentangled spectra yields abundances for more than a dozen elements in each star. Based on the secondary, the system metallicity is near solar: $[{\rm Fe/H}] = +0.01 \pm 0.06$. Lithium is detected in the secondary but not in the primary. A comparison with current stellar evolution models shows a good match to the measured properties at an age of about 1.1 Gyr.

Key words: binaries: eclipsing – stars: evolution – stars: fundamental parameters – stars: individual (V501 Mon) – techniques: photometric – techniques: spectroscopic

Supporting material: machine-readable and VO tables

1. INTRODUCTION

The eclipsing binary V501 Mon (with alternate names 2MASS J06404172−0106400 and TYC 4799-1943-1; $V = 12.32$, SpT A6m+F0 as determined here) was discovered by Wachmann (1966) in a photographic survey, and was given the original designation HBV 444. He proposed an orbital period of 7.021115 days, near the value we find below, and found a displaced secondary minimum indicating an eccentric orbit. A reexamination of the original plates was done by Bossen & Klawitter (1972), essentially confirming the original results, but with better precision. Since then, numerous times of eclipse have been published, and V501 Mon has been mentioned as a target worthy of followup for apsidal motion studies, possibly featuring an important contribution to the precession from General Relativity (Giménez 1985, 1995). Sebastian et al. (2012) classified V501 Mon as of spectral type A9 III. To date there has been no spectroscopic study of the system.

In this paper we present new differential photometry of V501 Mon as well as extensive high-resolution spectroscopy, the combination of which enables us to derive accurate absolute dimensions for the components as well as their chemical abundances for more than a dozen elements. As we describe below, the primary is found to be a metallic-line A star. Most such objects are members of binary systems (Abt 1961; Abt & Levy 1985). Among the dozen or so Am binaries with well determined properties, only a handful have been subjected to detailed abundance analyses (see Lyubimkov et al. 1996; Torres et al. 2012; Pavlovski et al. 2014); thus V501 Mon adds significantly to this class of objects, and may assist in understanding the Am phenomenon.

2. ECLIPSE TIMINGS

Measurements of the times of eclipse for V501 Mon collected from the literature are listed in Table 1, and cover approximately seven decades. An ephemeris curve solution using the method of Lacy (1992) gave clear indications of apsidal motion, as suspected by Giménez (1985), and resulted in a best fit eccentricity of $e = 0.1313 \pm 0.0019$, longitude of periastron $\omega = 231\overset{\circ}{.}54 \pm 0\overset{\circ}{.}71$, and reference epoch of primary minimum HJD 2,453,401.65029 ± 0.00060, where the inclination angle has been held fixed at the value determined from our light-curve fit below ($i = 88\overset{\circ}{.}022$). The apsidal period, however, is still very uncertain ($U = 16{,}000 \pm 11{,}000$ years), and strong correlations are present between the eccentricity and the rate of apsidal motion in this "unconstrained" solution. Given that the spectroscopic measurements we present below provide a stronger handle on *e*, a preferable approach is to perform a simultaneous fit of the eclipse timings and the radial velocities (RVs), which should constrain the parameters better. We defer a discussion of this solution until Section 4.

3. SPECTROSCOPIC OBSERVATIONS AND RVs

Spectroscopic observations of V501 Mon were carried out with three different instruments. They began at the Harvard-Smithsonian Center for Astrophysics (CfA) in 2005 November, using the now decommissioned Digital Speedometer (DS; Latham 1992) mounted on the 1.5 m Tillinghast reflector at the Fred L. Whipple Observatory on Mount Hopkins (AZ). Seven spectra were recorded through 2009 March with an intensified photon-counting Reticon detector, and cover a narrow span of 45 Å centered at 5190 Å (Mg I b triplet). The resolving power of this instrument was $R \approx 35{,}000$, and the signal-to-noise ratios of the spectra range from 13 to 22 per resolution element

Table 1
Times of Eclipse for V501 Mon

HJD (2,400,000+)	ϵ (days)	Eclipse	Type	$(O-C)$ (days)	Source
30077.2220	…	1	pg	+0.01762	1
30431.3800	…	2	pg	−0.01654	1
31077.3560	…	2	pg	+0.00819	1
31144.4230	…	1	pg	−0.00467	1
31144.4280	…	1	pg	+0.00033	1
31786.4970	…	2	pg	+0.00703	1
31846.5810	…	1	pg	+0.03275	1
33703.3080	…	2	pg	+0.02785	1
33710.3090	…	2	pg	+0.00764	1
34040.2580	…	2	pg	−0.04021	1
34068.3530	…	2	pg	−0.03005	1
34086.3060	…	1	pg	−0.00692	1
34086.3400	…	1	pg	+0.02708	1
34416.3070	…	1	pg	−0.00259	1
34444.4320	…	1	pg	+0.03758	1
34451.3920	…	1	pg	−0.02362	1
34767.3870	…	1	pg	+0.01711	1
34767.4250	…	1	pg	+0.05511	1
34770.4820	…	2	pg	−0.02199	1
34781.3920	…	1	pg	−0.02030	1
34781.4220	…	1	pg	+0.00970	1
34795.4210	…	1	pg	−0.03371	1
35107.5130	…	2	pg	−0.00905	1
35160.5080	…	1	pg	−0.04941	1
35160.5390	…	1	pg	−0.01841	1
52320.38766	0.0025	1	ccd	+0.00322	2
52983.5215	0.0002	2	ccd	+0.00009	3
53376.7091	0.0005	2	ccd	−0.00004	4
53390.7530	0.0006	2	ccd	+0.00144	4
53401.6502	0.0005	1	ccd	+0.00006	4
53404.7933	0.0005	2	ccd	−0.00068	4
53671.6010	0.0005	2	ccd	+0.00106	5
54422.8674	0.0005	2	ccd	−0.00195	6
54450.9531	0.0007	2	ccd	−0.00109	6
54454.8302	0.0004	1	ccd	−0.00081	6
54475.8934	0.0008	1	ccd	−0.00123	6
54787.9741	0.0006	2	ccd	+0.00185	6
54791.8490	0.0010	1	ccd	+0.00011	6
55135.8866	0.0019	1	ccd	−0.00137	7
55170.9960	0.0013	1	ccd	+0.00200	7
55493.9715	0.0009	1	ccd	+0.00203	7
55500.9939	0.0011	1	ccd	+0.00323	7
56339.65867	0.00026	2	ccd	−0.00088	8
56339.65954	0.00038	2	ccd	−0.00001	8
56339.66015	0.00022	2	ccd	+0.00060	8
56676.6771	0.0009	2	ccd	−0.00050	9

Note. Measurement errors (ϵ) are listed as published. "Eclipse" is 1 for a primary eclipse, 2 for a secondary eclipse. "Type" is pg for photographic measurements and ccd for more modern determinations. Uncertainties for the photographic measurements are estimated to be $\epsilon = 0.025$ days, as explained in Section 4. $O-C$ residuals are computed from the combined fit described there. Sources for the times of eclipse are: (1) http://var2.astro.cz/EN/brno/eclipsing_binaries.php; (2) Brát et al. (2007), (3) Measured from a minimum observed by M. Wolf (2015, private communication), (4) Lacy (2006), (5) Zejda et al. (2006), (6) Lacy (2009), (7) Lacy (2011), (8) Diethelm (2013), (9) Lacy (2014).

of 8.5 km s^{-1}. Dusk and dawn exposures of the sky were taken nightly to monitor the velocity zero point.

Thirty seven additional spectra were gathered from 2009 November to 2015 February with the Tillinghast Reflector Echelle Spectrograph (TRES; Fűrész 2008) on the same telescope. This bench-mounted, fiber-fed instrument provides a resolving power of $R \approx 44{,}000$ in 51 orders over the wavelength span 3900–9100 Å. The signal-to-noise ratios of the 37 spectra range from 8 to 56 per resolution element of 6.8 km s^{-1}. IAU RV standard stars were observed each night.

Between 2011 October and 2015 February we also obtained 57 usable spectra of V501 Mon with the Tennessee State University 2 m Automatic Spectroscopic Telescope (AST) and a fiber-fed echelle spectrograph (Eaton & Williamson 2007) at Fairborn Observatory in southeast Arizona. The detector for these observations was a Fairchild 486 CCD, with 15 μm pixels in a 4096 × 4096 format. The spectrograms have 48 orders ranging from 3800 to 8260 Å. Because of the faintness of V501 Mon ($V = 12.32$), we used a fiber that produced a spectral resolution of 0.4 Å, corresponding to a resolving power of 15000 at 6000 Å. See Fekel et al. (2013) for additional information about the AST facility. Our spectra have typical signal-to-noise ratios per resolution element of 40 at 6000 Å.

RVs from the CfA spectra were measured using the two-dimensional cross-correlation technique TODCOR (Zucker & Mazeh 1994), with synthetic templates taken from a large library of calculated spectra based on model atmospheres by R. L. Kurucz (see Nordström et al. 1994; Latham et al. 2002), restricted to the Mg I b region. Template parameters (effective temperature, surface gravity, metallicity, and rotational broadening) were selected by running grids of cross-correlations as described by Torres et al. (2002). We adopted initial surface gravities of $\log g = 4.0$, close to our final values in Section 7, and solar metallicity. Further experiments showed that while solar composition is favored for the secondary (star B), a better match to the observed spectra is achieved by adopting a metallicity for the primary (star A) of [Fe/H] = +0.5, which we have often seen in the past in objects with chemical peculiarities typical of Am stars. This was a first indication that the primary component of V501 Mon may be metallic-lined. The temperatures for the primary and secondary that maximize the cross-correlation coefficient averaged over all exposures are 7280 and 6950 K, although these are sensitive to the adopted metallicity and surface gravity and could be biased if the primary composition is anomalous. Formal uncertainties for these temperatures are 200 K each. The rotational broadenings were determined to be $v \sin i = 17 \pm 1$ km s^{-1} and 11 ± 2 km s^{-1}, respectively. The heliocentric velocities we obtained from the DS and TRES spectra were placed on a common frame and are listed in Table 2. Those from the DS include corrections for potential systematic effects due to the narrow spectral window (see Latham et al. 1996) determined from numerical simulations as described by Torres et al. (1997). These corrections are smaller than 0.5 km s^{-1} for both stars, and have little effect on the results presented later.

We determined the light ratio separately for the seven DS and the 37 TRES spectra following Zucker & Mazeh (1994), and obtained values of $\ell_B/\ell_A = 0.58 \pm 0.06$ and 0.53 ± 0.02, respectively, at a mean wavelength of 5190 Å. We point out, however, that these values are also sensitive to the metallicity and temperatures adopted for the cross-correlation templates, and may be biased if the composition of the primary is peculiar (which could in turn affect the temperature derived for this star). For example, using a primary temperature of 7500 K, closer to the value found below, reduces the light ratio from TRES to $\ell_B/\ell_A = 0.49 \pm 0.02$. Although a template mismatch

Table 2
Heliocentric Radial Velocity Measurements of V501 Mon from CfA

HJD (2,400,000+)	RV_A (km s^{-1})	ϵ_A (km s^{-1})	$(O-C)_A$ (km s^{-1})	RV_B (km s^{-1})	ϵ_B (km s^{-1})	$(O-C)_B$ (km s^{-1})	Orbital Phase	Instrument
53690.9255	−84.96	0.64	−0.42	84.73	2.32	+3.61	0.2002	DS
54048.9456	−82.16	0.47	+0.50	76.84	1.72	−2.16	0.1915	DS
54070.9780	−76.65	0.39	+0.10	72.80	1.40	+0.47	0.3295	DS
54136.8728	62.18	0.46	−0.45	−85.06	1.66	−0.16	0.7146	DS
54424.9270	60.25	0.37	−0.07	−82.04	1.32	+0.25	0.7409	DS

(This table is available in its entirety in machine-readable and Virtual Observatory (VO) forms.)

Table 3
Heliocentric Radial Velocity Measurements of V501 Mon from Fairborn Observatory

HJD (2,400,000+)	RV_A (km s^{-1})	ϵ_A (km s^{-1})	$(O-C)_A$ (km s^{-1})	RV_B (km s^{-1})	ϵ_B (km s^{-1})	$(O-C)_B$ (km s^{-1})	Orbital Phase
55864.835	46.10	0.69	−0.36	−65.50	1.26	+0.61	0.8207
55928.777	14.40	0.69	+0.05	−31.70	1.26	−1.81	0.9277
55945.678	−74.40	0.69	−0.03	71.40	1.26	+1.21	0.3348
55949.894	13.40	0.69	+1.76	−25.70	1.26	+1.14	0.9353
55958.876	−86.60	0.69	+0.03	85.70	1.26	+1.68	0.2145

(This table is available in its entirety in machine-readable and Virtual Observatory (VO) forms.)

may affect the derived temperatures and light ratio, experience has shown that it has little effect on $v \sin i$ or on the RVs.

Fekel et al. (2009) gave a general explanation of the velocity measurement from our Fairborn echelle spectra. For V501 Mon we have used our solar-type line list and measured velocities for the lines in that list that are just in the orders that cover the wavelength region 4920–7100 Å. Our velocities were determined by fitting the individual lines with rotational broadening functions (Lacy & Fekel 2011) that allowed both the depth and width of the line fits to vary. Our unpublished measurements of several IAU solar-type velocity standards show that these Fairborn Observatory velocities have a zero-point offset of -0.6 km s^{-1} when compared to the results of Scarfe (2010). Therefore, 0.6 km s^{-1} has been added to each velocity. We list the final values in Table 3.

From the solar-type line list for the AST spectra, the average projected rotational velocities of components A and B are 16.5 and 12.4 km s^{-1}. These $v \sin i$ values have an estimated uncertainty of 1 km s^{-1}.

4. SPECTROSCOPIC ORBITAL SOLUTION

Separate orbital solutions using the CfA and Fairborn velocities are listed in Table 4, and are generally consistent with each other. In order to optimally combine the information contained in the RVs and in the eclipse timings, we carried out a joint solution using the two RV data sets and the times of eclipse from Section 2, solving for the spectroscopic orbital elements and the apsidal motion simultaneously. The prescription for the latter is based on the algorithm of Lacy (1992). The long baseline of the eclipse timings helps to constrain the period, and the spectroscopic measurements constrain the orbital eccentricity, which is otherwise strongly correlated with the apsidal motion if using only the timings to determine $d\omega/dt$. Formal measurement uncertainties were used to establish weights, and adjusted iteratively during the solution so as to achieve reduced chi-squared values near unity, separately for the primary and secondary components and for each type of observation. For the photographic times of eclipse that have no published uncertainties our procedure assigned an average error of 0.025 days. Photoelectric/CCD timings with published errors in Table 1 were scaled by factors of 1.7 for the primary and 2.2 for the secondary. The inclination angle was held fixed according to the value determined from our light curve fit in Section 5. Tests show that its small error contributes negligibly to the uncertainties in all other adjusted quantities.

The results of our weighted least-squares fit are given in the last column of Table 4. Though improved over the preliminary value listed in Section 2, the apsidal motion period U remains relatively uncertain at 15,400 ± 8300 years. For each RV set we included as an adjustable parameter an offset between the zero points of the primary and secondary velocities, which for the CfA measurements may arise because of a template mismatch, or for other reasons. We also allowed for a possible overall shift between the Fairborn and CfA velocities. All of these shifts turn out to be small, but are statistically significant. We illustrate the solution for the spectroscopic elements in Figure 1, which shows the RV measurements and their $O-C$ residuals from the fit, separately for the Fairborn and CfA data sets. The residuals are listed in Tables 2 and 3. Those from the eclipse timings and the best-fit ephemeris curve are displayed in Figure 2.

5. DIFFERENTIAL PHOTOMETRY AND LIGHT CURVE SOLUTION

An extensive program of CCD photometry was carried out using the NFO WebScope (Grauer et al. 2008) near Silver City, New Mexico, for the purpose of gathering an accurate V-band light curve of V501 Mon for analysis. A total of 6729 images were obtained over 281 nights between 2005 January and February. Comparison stars (TYC 4799-1956-1 and TYC 4799-1098-1, with $V = 10.31$ and 11.21, respectively, both of spectral type A0) within 10 arcmin in the same field of view as the variable star were used to determine differential magnitudes. The magnitudes were corrected for nightly variations in the photometric zero point as we have done previously in similar studies (see, e.g., Lacy et al. 2008). The

Table 4
Spectroscopic/Ephemeris-curve Solutions for V501 Mon

Parameter	CfA	Fairborn	RVs + Timings
$P_{\rm sid}$ (days)	...	...	7.02120771 ± 0.00000097
$P_{\rm anom}$ (days)	7.021201 ± 0.000014	7.021254 ± 0.000061	7.0212164 ± 0.0000053
γ (km s^{-1})	−6.91 ± 0.11	−6.692 ± 0.099	−7.067 ± 0.045
$K_{\rm A}$ (km s^{-1})	76.914 ± 0.054	76.91 ± 0.12	76.866 ± 0.047
$K_{\rm B}$ (km s^{-1})	86.58 ± 0.13	87.22 ± 0.19	86.71 ± 0.11
e	0.1359 ± 0.0015	0.1348 ± 0.0015	0.13388 ± 0.00059
$\omega_{\rm A}$ at $T_{\rm min\ I}$ (deg)	232.19 ± 0.66	233.07 ± 0.65	232.43 ± 0.21
$T_{\rm min\ I}$ (HJD−2,400,000)	53401.6532 ± 0.0072	53401.633 ± 0.025	53401.65013 ± 0.00044
$T_{\rm peri}$ (HJD−2,400,000)	53404.224 ± 0.012	53404.227 ± 0.057	53404.2302 ± 0.0039
$d\omega/dt$ (deg cycle^{-1})	...	...	0.00045 ± 0.00024
U (yr)	...	...	15400 ± 8300
i (deg)	...	...	88.022 (fixed)
$M_{\rm A}\sin^3 i$ ($M_\odot$)	1.6374 ± 0.0049	1.6628 ± 0.0078	1.6426 ± 0.0043
$M_{\rm B}\sin^3 i$ ($M_\odot$)	1.4545 ± 0.0029	1.4663 ± 0.0054	1.4562 ± 0.0025
$a_{\rm A}\sin i$ (10^6 km)	7.3570 ± 0.0045	7.358 ± 0.011	7.3545 ± 0.0043
$a_{\rm B}\sin i$ (10^6 km)	8.282 ± 0.012	8.344 ± 0.018	8.296 ± 0.010
$a\sin i$ ($R_\odot$)	22.481 ± 0.019	22.571 ± 0.031	22.498 ± 0.016
$q \equiv M_{\rm B}/M_{\rm A}$	0.8883 ± 0.0013	0.8818 ± 0.0023	0.8865 ± 0.0012
ΔRV CfA (prim − sec) (km s^{-1})	−0.50 ± 0.25	...	−0.79 ± 0.13
ΔRV Fairborn (prim − sec) (km s^{-1})	...	−0.60 ± 0.20	−0.43 ± 0.18
ΔRV (CfA − Fairborn) (km s^{-1})	...	...	−0.426 ± 0.097
$\sigma_{\rm A}$ (km s^{-1})	0.26	0.64	0.28 / 0.64
$\sigma_{\rm B}$ (km s^{-1})	0.74	1.08	0.73 / 1.16
Time span (days)	3372.9	1207.9	26995.5
$N_{\rm RV}$	44	57	44 / 57
$N_{\rm ecl}$	...	...	46

Note. Symbols in the first column represent the sidereal and anomalistic periods, the center-of-mass velocity (which for the combined fit is on the CfA reference system), the velocity semi-amplitudes, eccentricity, longitude of periastron of the primary, reference time of primary eclipse, time of periastron passage, rate of apsidal motion, apsidal period, and inclination angle. The ΔRV entries represent offsets between the primary and secondary velocities in each data set (primary minus secondary), and an overall difference in the velocity zero points in the sense CfA minus Fairborn. The physical constants used here are those adopted by Torres (2010).

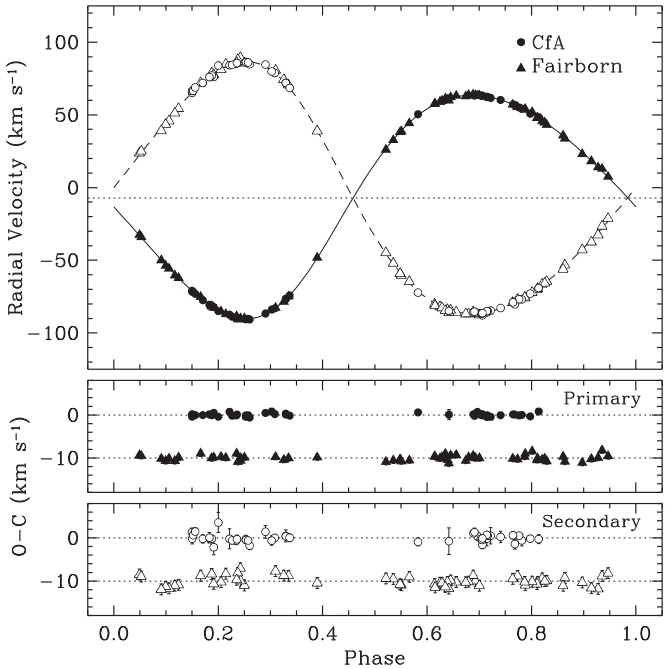

Figure 1. Spectroscopic orbital solution for V501 Mon along with the measurements. Primary velocities are shown with filled symbols, and the dotted line represents the center-of-mass velocity. The bottom panels display the residuals, with those from Fairborn Observatory displaced vertically for clarity.

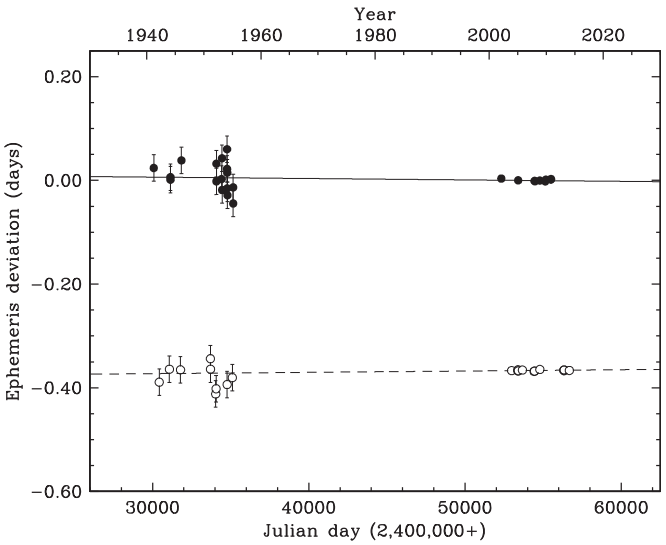

Figure 2. Ephemeris curve for V501 Mon from our combined orbital fit, along with the eclipse timing measurements. Primary measurements are shown with filled circles.

variable star differential magnitude was referenced to the magnitude of the combined light of the two comparison stars (variable minus comparisons) in each image. Table 5 lists these differential photometric measurements.

Table 5
Differential *V*-band Measurements of V501 Mon

HJD (2,400,000+)	ΔV (mag)
53376.65788	2.672
53376.66208	2.704
53376.66422	2.697
53376.66633	2.708
53376.66839	2.726

(This table is available in its entirety in machine-readable and Virtual Observatory (VO) forms.)

The *V*-band light curve of this well-detached system was analyzed using the JKTEBOP application of Southworth (2011) (see also Etzel 1981; Popper & Etzel 1981). This program can combine the brightness measurements with RV measurements and even historical eclipse timings, but does not currently take into account apsidal motion, nor can it use more than one RV set for each component. As mentioned earlier, the determination of $d\omega/dt$ benefits greatly when the eccentricity can be constrained by the spectroscopy. Consequently, we have elected to apply JKTEBOP to only the brightness measurements of V501 Mon, and to treat the RVs and eclipse timings separately, as already described in Sections 2 and 4. The fitted parameters from JKTEBOP and their uncertainties are given in Table 6, and are the central surface brightness of the secondary (J_B) in units of the primary, the sum of the relative radii ($r_A + r_B$), the radius ratio ($k \equiv r_B/r_A$), the inclination angle (i), the linear limb-darkening coefficients (u_A, u_B), the eccentricity (e), the longitude of periastron of the primary (ω_A), the sidereal period (P_{sid}), and a reference time of primary eclipse ($T_{Min\,I}$). The gravity darkening coefficients (y_A, y_B) were assumed to be the same for the two components and were held fixed at their theoretical values for radiative stars. The mass ratio was adopted from our spectroscopic orbit (Table 4). The normalized flux contributions of the stars (ℓ_A, ℓ_B) were computed internally by the program. Experiments in which we allowed for third light (ℓ_3) returned values not significantly different from zero. The eccentricity and ω_A from our fit are perfectly consistent with the much better determined values in Table 4. A graphical representation of the fitted model along with the observations appears in Figures 3–5.

6. ATMOSPHERIC PARAMETERS AND CHEMICAL COMPOSITION

In this section we describe our more detailed study of the atmospheric properties of the V501 Mon components, including their elemental abundances, that begins with a reconstruction of their individual spectra by the method of spectral disentangling (Simon & Sturm 1994). The method works best with a time series of high-resolution spectra more or less evenly distributed in orbital phase (Hensberge et al. 2008), as we have for V501 Mon. In its most general form this procedure can solve for the spectroscopic orbital elements in addition to the individual spectra, so in a sense it is a generalization of the technique of Doppler tomography (Bagnuolo & Gies 1991), in which the separation of the component spectra is made for a given set of known RVs for each star. In this case the orbit is already well known from our fit in Section 4, and the elements were held fixed, i.e., disentangling was performed in "pure separation" mode.

Table 6
Light-curve Solution for V501 Mon

Parameter	Value
J_B	0.738 ± 0.040
$r_A + r_B$	0.15456 ± 0.00057
r_A	0.0838 ± 0.0013
r_B	0.0707 ± 0.0013
$k \equiv r_B/r_A$	0.843 ± 0.027
i (deg)	88.022 ± 0.076
u_A	0.60 ± 0.11
u_B	0.51 ± 0.10
$y_A = y_B$	0.25 fixed
e	0.1296 ± 0.0054
ω_A (deg)	231.0 ± 2.0
ℓ_3	0 fixed
ℓ_A	0.648 ± 0.020
ℓ_B	0.352 ± 0.023
ℓ_B/ℓ_A	0.544 ± 0.036
P_{sid} (days)	7.02120688 ± 0.00000050
$T_{min\,I}$ (HJD−2,400,000)	53401.64906 ± 0.00016
σ (mmag)	13.5980
N	6729

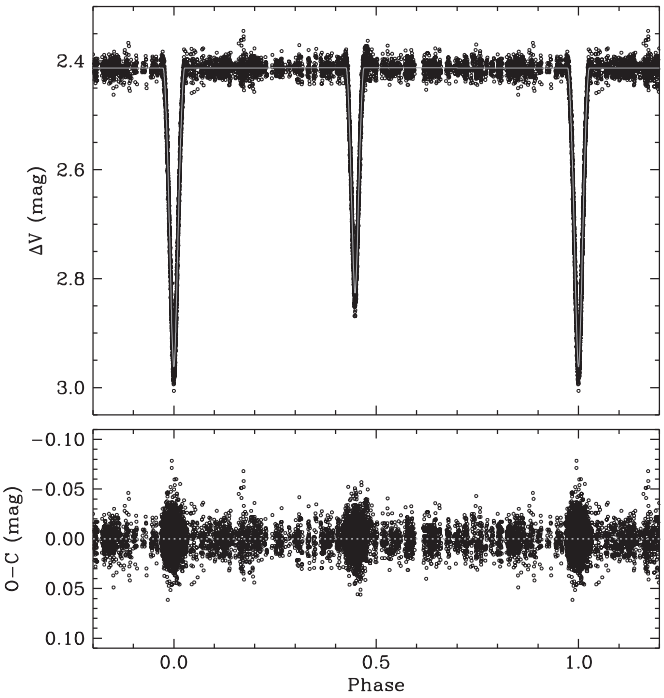

Figure 3. NFO differential *V*-band observations of V501 Mon, shown with our best model fit. Residuals from the fit are shown at the bottom.

For this work we used the disentangling code FDBinary (Ilijić et al. 2004), which operates in Fourier space based on the prescription of Hadrava (1995), with some improvements. The Fast Fourier Transform implemented in FDBinary gives more flexibility in selecting the edges of the spectral segments for disentangling, preserving the original spectral resolution. The choice of where to place the edges of each segment is a critical step in Fourier-type disentangling as these points should be strictly on the continuum. Errors incurred in selecting the edges in spectra with a high density of lines or with significant

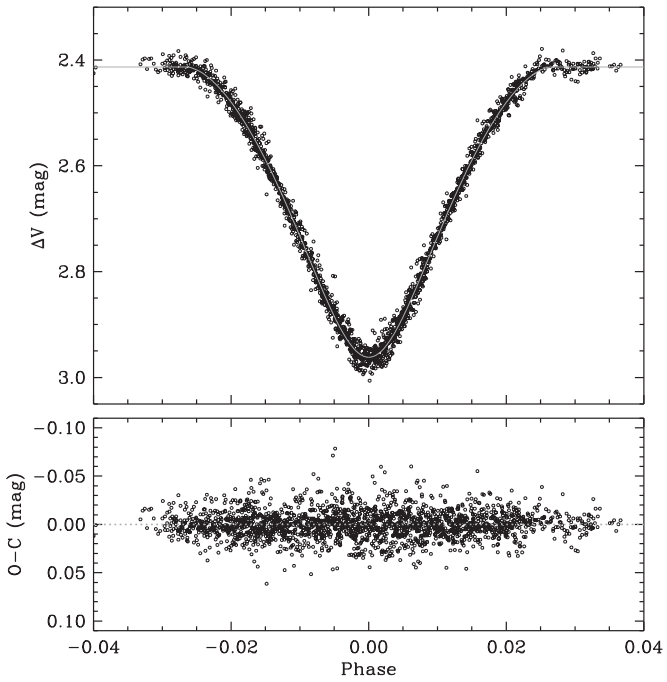

Figure 4. Enlargement of Figure 3 around the primary minimum.

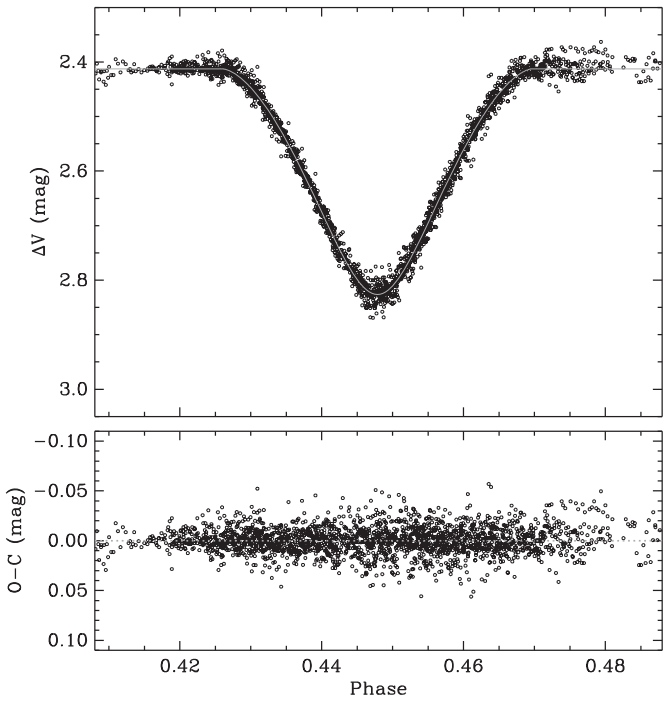

Figure 5. Enlargement of Figure 3 around the secondary minimum.

rotational broadening can add unwanted undulations in the disentangled spectra of the components.

We ran `FDBinary` on 27 of our TRES spectra of V501 Mon with the highest signal-to-noise ratios (averaging about 22 pixel^{-1}), still retaining good phase coverage. Since imperfections in the normalization of the echelle spectra are another potential source of spurious undulations, we performed the disentangling in relatively short spectral segments, usually 100–150 Å wide. The full spectral range we analyzed is 4000–6760 Å, corresponding to about 30,500 pixels.

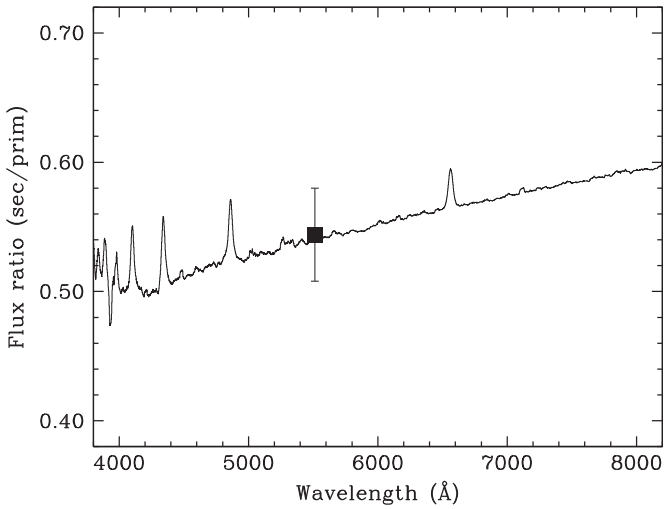

Figure 6. Flux ratio for V501 Mon computed from synthetic spectra with parameters near those of the components ($T_{\rm eff}$ = 7500 K, log g = 4.0, and [Fe/H] = +0.5 for the primary, and $T_{\rm eff}$ = 7000 K, log g = 4.0, and [Fe/H] = 0.0 for the secondary), and the measured radius ratio k = 0.843. The V-band value estimated from our light curve fit ($\ell_{\rm B}/\ell_{\rm A}$; Table 6) is also shown.

In the absence of a significant variation in the relative line strengths of the components as a function of orbital phase there is an ambiguity in the determination of the intrinsic line strengths for each star. In other words, the disentangled spectra remain in the common continuum of the total light of the binary system, and renormalization to their individual continua requires external information, such as light ratios inferred directly from the light-curve fit of an eclipsing binary (e.g., Hensberge et al. 2000; Pavlovski & Hensberge 2005). For V501 Mon we have this (Table 6), but effectively only at a single wavelength corresponding to the center of the V band. In order to estimate the flux ratio at other wavelengths we used synthetic spectra based on PHOENIX models (Husser et al. 2013) with parameters near those in Table 8 below, and we adopted the measured radius ratio k from Table 6. Figure 6 shows the result, which is in good agreement with the measured light ratio in V. Therefore, for renormalization purposes we used a smoothed version of this predicted relation.

Figure 7 shows a sample section of the disentangled spectra for the primary and secondary of V501 Mon (second and third from the top) on the common continuum of the composite spectrum of the binary (top). Also shown at the bottom are the same spectra renormalized according to the relation described above from Figure 6. The signal-to-noise ratios of the reconstructed spectra are 73 and 39 pixel^{-1} for the primary and secondary, respectively, at a mean wavelength of 5500 Å.

Next we used these disentangled spectra to infer the stellar parameters and abundances. Effective temperature and microturbulence $\xi_{\rm t}$ were determined from the numerous iron lines, and the usual conditions of excitation balance and null correlation of the iron abundance with the reduced equivalent widths, respectively, iterating as necessary. Equivalent widths of the Fe I and Fe II lines carefully selected from the line list of Bruntt et al. (2012) were measured with the `UCLSYN` code (Smalley et al. 2001), which was also used for the calculation of the theoretical spectra. The surface gravities of the stars are well known from our spectroscopic and light-curve solutions and were held fixed at the values reported later in Table 8. Initial results clearly indicated an enhanced metallicity for the

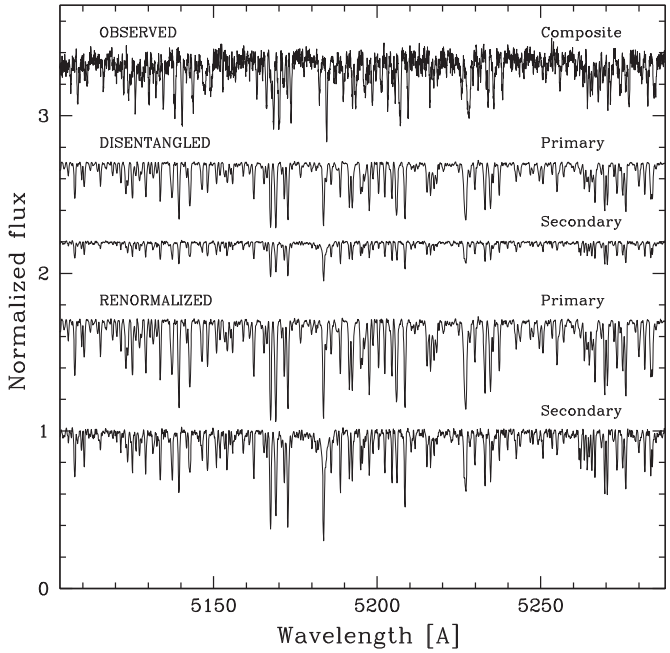

Figure 7. Portions of the disentangled spectra of V501 Mon before and after normalization. From top to bottom the figure shows one of our composite spectra, the reconstructed primary and secondary spectra on the common continuum of the binary, and the same two spectra after normalization.

primary consistent with earlier indications of an Am nature, with [Fe/H] $\sim +0.30$. We therefore adjusted our atmosphere model accordingly, and repeated the analysis. The resulting excitation temperatures and microturbulence velocities based on the Fe I lines are $T_{\rm eff} = 7540 \pm 140$ K and $\xi_{\rm t} = 3.1 \pm 0.1$ km s^{-1} for the primary, and $T_{\rm eff} = 6960 \pm 110$ K and $\xi_{\rm t} = 1.3 \pm 0.1$ km s^{-1} for the secondary. The $\xi_{\rm t}$ value for the primary is consistent with results for normal A stars of this temperature (e.g., Kunzli & North 1998; Gebran et al. 2010, 2014), while that of the secondary seems slightly lower than in other stars of its type.

With both Fe I and Fe II lines being present in the spectra of the V501 Mon components, the effective temperatures can in principle also be derived from the condition of ionization balance, in which the strength of the singly ionized Fe lines is influenced by log g as well. However, with log g fixed as we described above, the iron abundances from Fe I and Fe II in each star are already in excellent agreement (and are A(Fe I) = 7.83 $\pm$ 0.07 and A(Fe II) = 7.80 $\pm$ 0.08 for the primary, and A(Fe I) = 7.51 $\pm$ 0.05 and A(Fe II) = 7.50 $\pm$ 0.07 for the secondary),[6] indicating no need to adjust the $T_{\rm eff}$ values since they already satisfy ionization balance.

Additional estimates of the temperatures were derived by fitting the wings of the Hα and Hβ line profiles with the STARFIT code (Tamajo et al. 2011; Kolbas et al. 2014), which performs an optimization based on a genetic algorithm (Charbonneau 1995). For this we used a precalculated grid of theoretical spectra in local thermodynamical equilibrium (for details, see Kolbas et al. 2014, 2015). The metal lines superimposed on the wings were masked out. The surface gravities and projected rotational velocities (see below) were held fixed, and uncertainties in the derived temperatures were calculated with a Markov Chain Monte Carlo technique (K. Pavlovski et al. 2015, in preparation). The results from the Hα lines are 7420 $\pm$ 140 K for the primary and 6790 $\pm$ 180 K for the secondary, and from the Hβ lines they are 7480 $\pm$ 150 K and 7070 $\pm$ 160 K, respectively. The latter results are consistent with our earlier estimates from the iron lines, while the Hα values are somewhat lower, as expected from the shallower depth of formation of this line.

Abundances for individual elements were derived using lines with the most reliable log gf values, and are listed in Table 7. The quoted uncertainties take account of the intrinsic scatter from the lines used in each case, as well as the uncertainties in $T_{\rm eff}$, log g, and $\xi_{\rm t}$. An additional contribution has been added to the error budget corresponding to a 1.5% error in the light ratio of V501 Mon. The results in Table 7 are on the solar abundance scale of Asplund et al. (2009). The abundance pattern of the two components is compared in Figure 8. While the secondary is seen to have solar composition within the uncertainties, the pattern for the primary is typical of Am stars, with a clear underabundance of Ca and Sc, an enhancement of the iron group elements, and a large overabundance of Ba and other heavy elements (Preston 1974).

The Li 6707 Å line is clearly visible in the spectrum of the secondary star. Line fitting yields an abundance estimate of A(Li) = 3.17 $\pm$ 0.16, in which the principal contribution to the uncertainty is from the error in the effective temperature. This abundance is consistent with that expected for stars of this mass and temperature (see, e.g., Ramírez et al. 2012). On the other hand, we find no trace of the Li line in the primary star spectrum. We can only place a rough upper limit of about A(Li) = 2.80.

Finally, we also made an estimate of the macroturbulence velocities ($\zeta_{\rm RT}$) and projected rotational velocities from the disentangled spectra. For the primary we obtained $\zeta_{\rm RT} = 6.3 \pm 1.6$ km s^{-1} and $v \sin i = 18.4 \pm 1.0$ km s^{-1}, and for the secondary $\zeta_{\rm RT} = 5.3 \pm 1.2$ km s^{-1} and $v \sin i = 15.4 \pm 0.9$ km s^{-1}.

7. ABSOLUTE DIMENSIONS

The combination of the spectroscopic and light-curve elements yields absolute masses for V501 Mon with relative errors of only 0.3% and 0.2% for the primary and secondary, and radius errors of 1.5% and 1.8%, respectively. Of the temperature determinations in the preceding section based on the disentangled TRES spectra, we adopt for each star a weighted average of the results from the metal lines and from Hβ, which are $T_{\rm eff}^{\rm A} = 7510 \pm 100$ K and $T_{\rm eff}^{\rm B} = 7000 \pm 90$ K. These correspond approximately to spectral types of A6 and F0. The Hα estimates are not considered for the reason mentioned above. The measured primary/secondary temperature difference, $\Delta T_{\rm eff} = 510 \pm 130$ K, is in very good agreement with the value 480 $\pm$ 140 K inferred directly from the light curves through the fitted central surface brightness parameter $J_{\rm B}$ and the visual absolute flux calibration of Popper (1980). We assume in the following that the chemical composition of the system is represented by the measured abundance for the secondary, given that the primary is anomalous. Thus, [Fe/H] = +0.01 $\pm$ 0.06, based on the numerous Fe I lines.

The physical properties of the components are collected in Table 8. For the distance estimate we adopted an apparent

[6] We use the standard abundance notation in which A(X) = log[n(X)/n(H)] + 12, where n(X) and n(H) are the numbers of atoms per unit volume of element X and of hydrogen.

Table 7
Abundances from Our Disentangled TRES Spectra of V501 Mon

		Primary			Secondary			
A	X	Abundance	[X/H]	N	Abundance	[X/H]	N	log $\epsilon_{\odot}$
11	Na I	…	…	…	6.28 ± 0.05	+0.04 ± 0.06	6	6.24 ± 0.04
12	Mg I	7.76 ± 0.07	+0.16 ± 0.08	3	7.52 ± 0.14	−0.08 ± 0.15	4	7.60 ± 0.04
14	Si I	7.64 ± 0.09	+0.13 ± 0.09	11	7.52 ± 0.07	+0.01 ± 0.08	5	7.51 ± 0.03
20	Ca I	…	…	…	6.33 ± 0.09	−0.01 ± 0.10	9	6.34 ± 0.04
20	Ca II	5.85 ± 0.08	−0.49 ± 0.09	6	…	…	…	6.34 ± 0.04
21	Sc II	2.52 ± 0.08	−0.63 ± 0.09	3	3.11 ± 0.04	−0.04 ± 0.06	6	3.15 ± 0.04
22	Ti I	5.40 ± 0.05	+0.45 ± 0.07	10	4.93 ± 0.09	−0.02 ± 0.10	15	4.95 ± 0.05
22	Ti II	5.31 ± 0.06	+0.36 ± 0.08	11	…	…	…	4.95 ± 0.05
24	Cr I	6.04 ± 0.09	+0.40 ± 0.10	15	5.63 ± 0.06	−0.01 ± 0.07	44	5.64 ± 0.04
24	Cr II	6.05 ± 0.08	+0.41 ± 0.09	9	5.61 ± 0.07	−0.03 ± 0.08	19	5.64 ± 0.04
25	Mn I	5.60 ± 0.11	+0.17 ± 0.12	7	5.36 ± 0.06	−0.07 ± 0.08	10	5.43 ± 0.05
26	Fe I	7.83 ± 0.07	+0.33 ± 0.08	159	7.51 ± 0.05	+0.01 ± 0.06	126	7.50 ± 0.04
26	Fe II	7.80 ± 0.08	+0.30 ± 0.09	18	7.50 ± 0.07	+0.00 ± 0.08	14	7.50 ± 0.04
27	Co I	…	…	…	5.05 ± 0.07	+0.06 ± 0.10	12	4.99 ± 0.07
28	Ni I	6.69 ± 0.08	+0.47 ± 0.09	41	6.22 ± 0.07	+0.00 ± 0.08	36	6.22 ± 0.04
39	Y II	…	…	…	2.17 ± 0.08	−0.04 ± 0.09	6	2.21 ± 0.05
56	Ba II	3.94 ± 0.11	+1.76 ± 0.14	3	…	…	…	2.18 ± 0.09

Note. Columns list the atomic number, the element and ionization degree, the logarithm of the number abundance on the usual scale in which A(H) = 12, the logarithmic abundance relative to the Sun, and the number of spectral lines measured. The last column gives the reference photospheric solar values from Asplund et al. (2009).

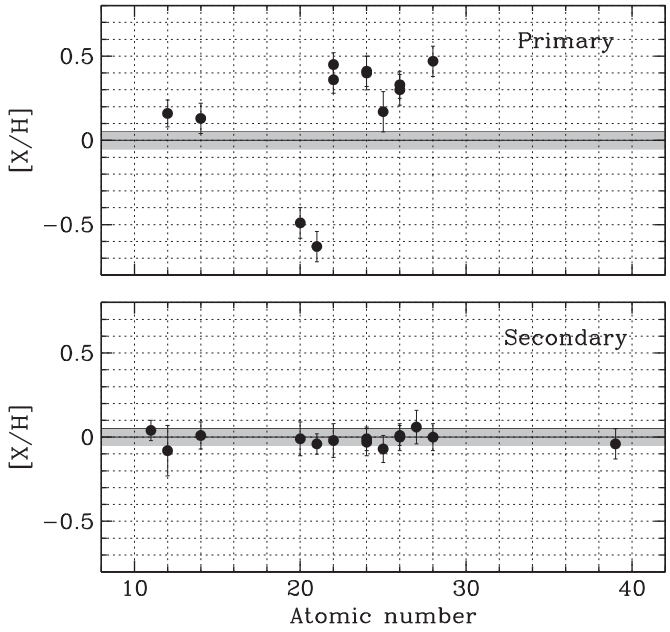

Figure 8. Measured abundances for the primary and secondary of V501 Mon. The abundance of Ba II for the primary star is not displayed, as it is far off the scale (+1.76, atomic number 56). For reference, the shaded area indicates the standard solar composition of Asplund et al. (2009).

visual magnitude $V = 12.320 \pm 0.020$ from the AAVSO Photometric All-sky Survey (Henden et al. 2012), along with the absolute luminosities and bolometric corrections from Flower (1996). The interstellar extinction toward V501 Mon, $A_V = 0.55 \pm 0.12$, was derived by iterations from the recent three-dimensional reddening map of Green et al. (2015) based on Pan-STARRS 1 and 2MASS photometry, and assuming $A_V = 3.1\ E(B-V)$. The resulting distance, $D = 1030 \pm 80$ pc, is very similar to an independent calculation relying on the visual surface fluxes (see Popper 1980), which gives $D = 1050 \pm 70$ pc.

Table 8
Physical Properties of V501 Mon

Parameter	Primary	Secondary
Mass ($M_{\odot}$)	1.6455 ± 0.0043	1.4588 ± 0.0025
Radius ($R_{\odot}$)	1.888 ± 0.029	1.592 ± 0.028
log g (cgs)	4.103 ± 0.013	4.199 ± 0.016
Temperature (K)	7510 ± 100	7000 ± 90
log $L/L_{\odot}$	1.007 ± 0.027	0.743 ± 0.043
BC_V[a]	0.03 ± 0.10	0.03 ± 0.10
$M_{\rm bol}$ (mag)[b]	2.215 ± 0.067	2.87 ± 0.11
M_V (mag)	2.18 ± 0.12	2.84 ± 0.15
F_V[c]	3.8749 ± 0.0057	3.846 ± 0.010
A_V (mag)	0.55 ± 0.12	
Distance (pc)[d]	1030 ± 80	
$m - M$ (mag)	10.06 ± 0.16	
$v_{\rm peri}$ sin i	18.0 ± 0.3	15.1 ± 0.3
$v_{\rm psync}$ sin i	15.1 ± 0.2	12.7 ± 0.2
Measured v sin i[e]	16.6 ± 1.0	11.2 ± 2.0
Measured v sin i[f]	18.4 ± 1.0	15.4 ± 0.9
Measured v sin i[g]	16.5 ± 1.0	12.4 ± 1.0
ξ_t (km s^{-1})	3.1 ± 0.1	1.3 ± 0.1
ζ_{RT} (km s^{-1})	6.3 ± 1.6	5.3 ± 1.2
[Fe/H] (dex)	+0.01 ± 0.06	
A(Li 6707 Å) (dex)	<2.80	3.17 ± 0.16

Notes.
[a] Bolometric corrections from Flower (1996).
[b] Uses $M_{\rm bol}^{\odot} = 4.732$ (see Torres 2010).
[c] Visual absolute flux (Popper 1980).
[d] Relies on the luminosities and bolometric corrections.
[e] Based on the original (composite) TRES spectra, determined from cross-correlation grids.
[f] Based on the disentangled TRES spectra.
[g] Based on the Fairborn spectra.

Table 8 lists the predicted rotational velocities of the stars under the assumption that tidal forces have synchronized them with the orbital motion at periastron ($v_{\rm peri}$ sin i), and the

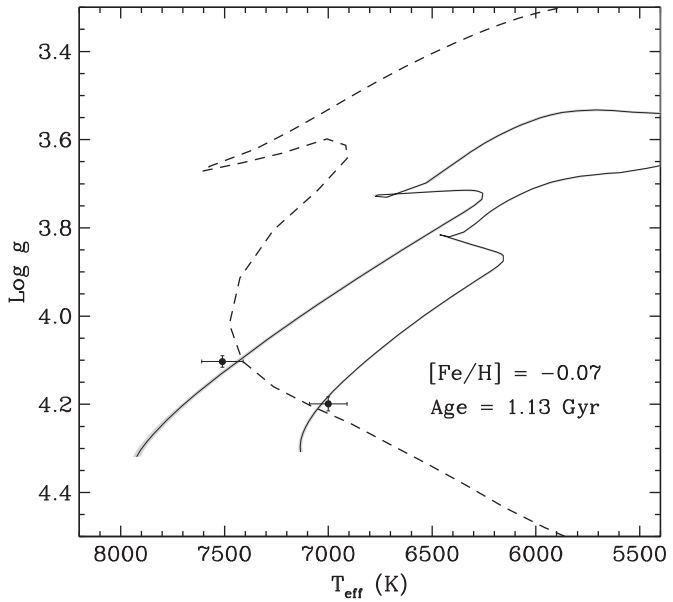

Figure 9. Stellar evolution models from the Yonsei-Yale series compared against the observations for V501 Mon. Evolutionary tracks (solid lines) are shown for the exact masses we measure, and for the metallicity that produces the best match, which is near the measured value. The very small mass errors mean that the uncertainty in the placement of the tracks is very small (indicated in the plot with a barely visible shaded region around each track). The best-fit isochrone shown by the dashed line has an age of 1.13 Gyr.

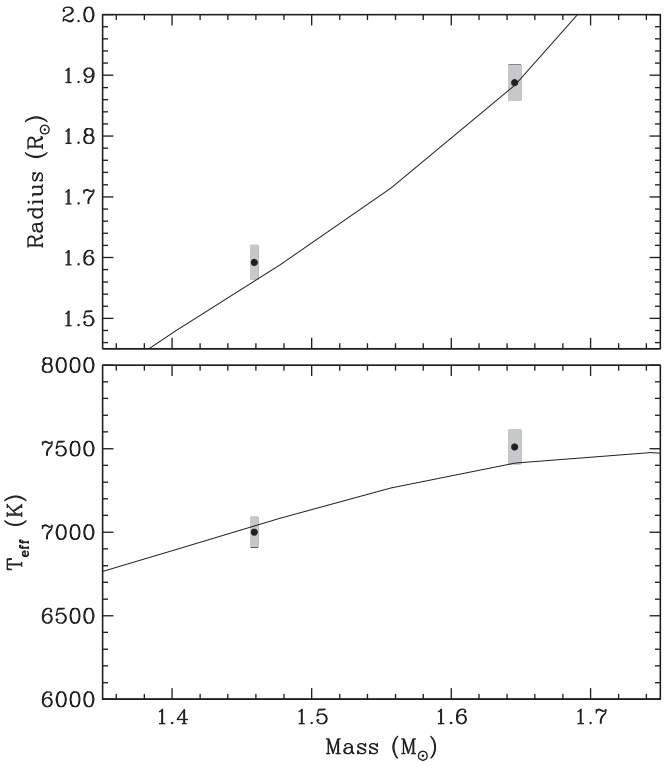

Figure 10. Mass–radius and mass–temperature diagrams showing the reference isochrone from Figure 9 ([Fe/H] = −0.07, 1.13 Gyr). The error boxes represent the observational uncertainties for V501 Mon.

alternate assumption that they are pseudo-synchronized ($v_{\rm psync}$ sin i; Hut 1981).[7] Slight disagreements between our three estimates of v sin i from Sections 3 and 6 prevent us from distinguishing between the two possibilities for V501 Mon. In particular, the two non-independent determinations from our CfA/TRES spectra differ by about twice their combined errors for the secondary component. Weight-averaging them, and then combining the result with the Fairborn estimates for each star yields mean v sin i values of 17.1 ± 0.7 and 12.8 ± 1.2 km s^{-1}, although we suspect systematic errors are not negligible.

8. COMPARISON WITH STELLAR EVOLUTION MODELS

Figure 9 presents a simultaneous comparison of the masses, radii, and temperatures of the V501 Mon components with stellar evolution models from the Yonsei-Yale series (Yi et al. 2001; Demarque et al. 2004). The solid lines correspond to evolutionary tracks for the exact masses we measure, beginning at the zero-age main sequence (ZAMS). The (solar-scaled) chemical composition of the models has been adjusted to reproduce the observations, and the best match is achieved for [Fe/H] $= -0.07$, which is not far from the measured value of [Fe/H] $= +0.01 \pm 0.06$. An isochrone for this metallicity and the best-fit age of 1.13 Gyr is shown with a dashed line. The stars are seen to be slightly evolved from the ZAMS. The radii and temperatures are shown separately as a function of mass in Figure 10, and compared against the same best-fit model isochrone. The agreement is very good.

The difference between the best-fit metallicity from the models and the measured composition of V501 Mon corresponds to about 1.3 times the uncertainty. If due to observational error in the temperatures and/or composition, one possible source for the small discrepancy is a bias in the light ratio we have adopted for the renormalization of the disentangled TRES spectra. The adopted dependence of the light ratio with wavelength relies on synthetic spectra for normal stars from Husser et al. (2013), which for the primary may differ from the true spectrum in subtle ways because of the Am nature of that star.

9. DISCUSSION AND CONCLUDING REMARKS

The high-precision masses and radii derived here for the detached, double-lined eclipsing binary V501 Mon place it in the elite group of systems with the best determined properties (e.g., Torres et al. 2010). Our detailed chemical analysis adds special value as fewer than three dozen of the systems with masses and radii known to better than 3% have been subjected to this type of study. The discovery that the primary is a metallic-line A star makes it an important object that may help us understand more about this phenomenon. So far as we are aware, only four other eclipsing binary systems with similarly well measured masses and radii have been published in which one or both components are Am/Fm stars, and which also have detailed element-by-element abundance analyses: β Aur (Lyubimkov et al. 1996), SW CMa and HW CMa (Torres et al. 2012), and YZ Cas (Pavlovski et al. 2014).

Figure 11 shows all well-studied (σ_M and σ_R less than 3%) A- and F-type stars in the field that are in the temperature range of V501 Mon from the compilation of Torres et al. (2010), with additions from the recent literature. Metallic-line stars are indicated with filled circles, and V501 Mon is represented with squares. Numerous studies in the literature have investigated the properties of Am/Fm stars in the field or in clusters. A connection has been sought between abundance patterns in

[7] Both scenarios also assume the stars' spin axes are parallel to the orbital axis.

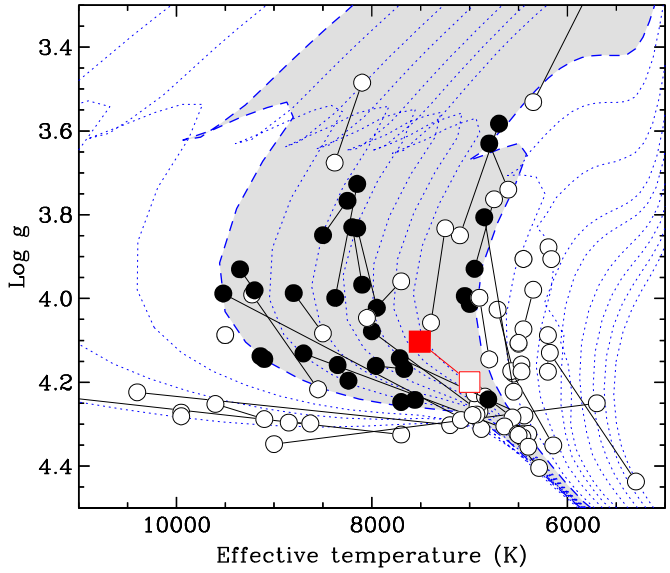

Figure 11. Field eclipsing binaries (circles) with well determined masses and radii in the temperature range of V501 Mon (squares). Solid lines connect components of the same binary, and metallic-line stars are indicated with filled symbols. Solar-metallicity isochrones from the Yonsei-Yale series (0.1–13 Gyr) are shown with dotted lines for reference. The dashed lines delimit the age range 0.4–1.5 Gyr within which the Am/Fm stars in this sample fall.

these objects and various characteristics such as binary orbital period or eccentricity, rotation, temperature, age, and others (e.g., Budaj 1996, 1997, 1999; Kunzli & North 1998; Abt 2000; Feňovčík et al. 2004; North & Debernardi 2004; Prieur et al. 2006, and references therein), but generally without an accurate knowledge of the basic stellar properties (mass, radius) or the age, which may be important if the anomalies depend sensitively on them. Only seven of the points in Figure 11 (from V501 Mon and the four systems mentioned earlier) have detailed photospheric abundances and many more may be needed before firm correlations can begin to be discerned as a function of mass, radius, or perhaps age. For now, the figure shows that the currently well-measured Am/Fm systems in the field are confined to the age range from about 0.4 to 1.5 Gyr (indicated with dashed lines), whereas normal A or F stars can be younger or older. The upper boundary also corresponds to a roughly constant temperature of 6700–6800 K. Kunzli & North (1998) found similar limits for field stars. Younger Am stars do of course exist in open clusters, such as the handful of examples in the Pleiades (Abt & Levato 1978; Burkhart & Coupry 1997; Hui-Bon-Hoa & Alecian 1998; Gebran & Monier 2008), and perhaps even among pre-main-sequence stars such as AK Sco (Herbig 1960; Andersen et al. 1989) with an age of only ∼18 Myr (Czekala et al. 2015).

We detect Li in the spectrum of the secondary of V501 Mon but not in the Am primary. Some studies have suggested that the Li abundance in Am stars is lower than in normal A stars by about a factor of 3 (e.g., Burkhart & Coupry 2000), while others have found no significant difference (e.g., Catanzaro & Ripepi 2014). In the 1.1 Gyr system V501 Mon the equal-age components do differ by at least a factor of 2, though it is unclear whether this may be more related to the temperature difference ($\Delta T_{\rm eff} \approx 500$ K in this case).

Finally, the measurement of apsidal motion in eclipsing binary systems has long been used to test models of the internal structure of stars (for a recent review, see Claret & Giménez 2010), specifically, the degree of mass concentration toward the center. In addition to the classical contributions to $d\omega/dt$ from tidal and rotational distortions, in a few systems the contribution from General Relativity (Levi-Civita 1937) is very important. This happens to be the case for V501 Mon, for which we calculate $(d\omega/dt)_{\rm GR} = 0.^\circ00032\ {\rm cycle}^{-1}$. Although the total measured apsidal motion is still very uncertain ($d\omega/dt = 0.^\circ00045 \pm 0.^\circ00024\ {\rm cycle}^{-1}$), the GR term appears to dominate, as anticipated by Giménez (1985), nominally contributing about 70% to the total amount. The internal structure constants for the primary and secondary of V501 Mon from the models by Claret (2004), $\log k_2 = -2.51$ and -2.42, lead to a predicted total apsidal motion rate (including the GR term) of $(d\omega/dt)_{\rm tot} = 0.^\circ00046\ {\rm cycle}^{-1}$ that is very close to the measured value.

We are grateful to P. Berlind, W. Brown, M. Calkins, G. Esquerdo, D. Latham, A. Milone, R. Stefanik, S. Tang, and S. Quinn for help in obtaining the CfA observations of V501 Mon with the DS and with TRES, and to R. J. Davis and J. Mink for maintaining the CfA echelle databases over the years. M. Wolf kindly provided his photometric measurements of a secondary eclipse of V501 Mon. The authors also wish to thank Bill Neely, who operates and maintains the NFO WebScope for the Consortium, and who handles preliminary processing of the images and their distribution. G. T. acknowledges partial support for this work from NSF grant AST-1509375. The work of KP has been supported in part by the Croatian Science Foundation under grant 2014-09-8656. NSF grant 1039522 from the Major Research Instrumentation Program, which was awarded to Tennessee State University, enabled the acquisition of the Fairborn observations. In addition, astronomy at Tennessee State is supported by the state of Tennessee through its Centers of Excellence program. This research has made use of the SIMBAD and VizieR databases, operated at CDS, Strasbourg, France, and of NASA's Astrophysics Data System Abstract Service.

REFERENCES

Abt, H. A. 1961, ApJS, 6, 37
Abt, H. A. 2000, ApJ, 544, 933
Abt, H. A., & Levato, H. 1978, PASP, 90, 201
Abt, H. A., & Levy, S. G. 1985, ApJS, 59, 229
Andersen, J., Lindgren, H., Hazen, M. L., & Mayor, M. 1989, A&A, 219, 142
Asplund, M., Grevesse, N., Sauval, A. J., & Scott, P. 2009, ARA&A, 47, 481
Bagnuolo, W. G., Jr., & Gies, D. R. 1991, ApJ, 376, 266
Bossen, H., & Klawitter, P. 1972, AcA, 22, 411
Brát, L., Zejda, M., & Svoboda, P. 2007, B.R.N.O. Contrib. 34, 1
Bruntt, H., Basu, S., Smalley, B., et al. 2012, MNRAS, 423, 122
Budaj, J. 1996, A&A, 313, 523
Budaj, J. 1997, A&A, 326, 655
Budaj, J. 1999, MNRAS, 310, 419
Burkhart, C., & Coupry, M. F. 1997, A&A, 318, 870
Burkhart, C., & Coupry, M. F. 2000, A&A, 354, 216
Catanzaro, G., & Ripepi, V. 2014, MNRAS, 441, 1669
Charbonneau, P. 1995, ApJS, 101, 309
Claret, A. 2004, A&A, 424, 919
Claret, A., & Giménez, A. 2010, A&A, 519, A57
Czekala, I., Andrews, S. M., Jensen, E. L. N., et al. 2015, ApJ, 806, 154
Demarque, P., Woo, J.-H., Kim, Y.-C., & Yi, S. K. 2004, ApJS, 155, 667
Diethelm, R. 2013, IBVS, 6063
Eaton, J. A., & Williamson, M. H. 2007, PASP, 119, 886

Etzel, P. B. 1981, in Proc. NATO Adv. Study Inst., Photometric and Spectroscopic Binary Systems, ed. E. B. Carling & Z. Kopal (Dordrecht: Reidel), 111
Fekel, F. C., Rajabi, S., Muterspaugh, M. W., & Williamson, M. H. 2013, AJ, 145, 111
Fekel, F. C., Tomkin, J., & Williamson, M. H. 2009, AJ, 137, 3900
Feňovčík, M., Budaj, J., Iliev, I., Richards, M. T., & Barzova, I. 2004, in IAU Symp. 224, The A-Star Puzzle, ed. J. Zverko et al. (Cambridge: Cambridge Univ. Press), 749
Flower, P. J. 1996, ApJ, 469, 355
Fűrész, G. 2008, PhD thesis, Univ. Szeged
Gebran, M., & Monier, R. 2008, A&A, 483, 567
Gebran, M., Monier, R., Royer, F., Lobel, A., & Blomme, R. 2014, in Putting A Stars into Context: Evolution, Environment, and Related Stars, ed. G. Mathys et al. (Moscow: Pero Publishing House), 193
Gebran, M., Vick, M., Monier, R., & Fossati, L. 2010, A&A, 523, A71
Giménez, A. 1985, ApJ, 297, 405
Giménez, A. 1995, ExA, 5, 91
Grauer, A. D., Neely, A. W., & Lacy, C. H. S. 2008, PASP, 120, 992
Green, G. M., Schlafly, E. F., Finkbeiner, D. P., et al. 2015, ApJ, 810, 25
Hadrava, P. 1995, A&AS, 114, 393
Henden, A. A., Levine, S. E., Terrell, D., Smith, T. C., & Welch, D. 2012, JAVSO, 40, 430
Hensberge, H., Ilijić, S., & Torres, K. B. V. 2008, A&A, 482, 1031
Hensberge, H., Pavlovski, K., & Verschueren, W. 2000, A&A, 358, 553
Herbig, G. H. 1960, ApJ, 131, 632
Hui-Bon-Hoa, A., & Alecian, G. 1998, A&A, 332, 224
Husser, T.-O., Wende-von Berg, S., Dreizler, S., et al. 2013, A&A, 553, A6
Hut, P. 1981, A&A, 99, 126
Ilijić, S., Hensberge, H., Pavlovski, K., & Freyhammer, L. S. 2004, in ASP Conf. Ser. 318, Spectroscopically and Spatially Resolving the Components of the Close Binary Stars, ed. R. W. Hilditch, H. Hensberge & K. Pavlovski (San Francisco, CA: ASP), 111
Kolbas, V., Dervişoğlu, A., Pavlovski, K., & Southworth, J. 2014, MNRAS, 444, 3118
Kolbas, V., Pavlovski, K., Southworth, J., et al. 2015, MNRAS, 451, 4150
Kunzli, M., & North, P. 1998, A&A, 330, 651
Lacy, C. H. S. 1992, AJ, 104, 2213
Lacy, C. H. S. 2006, IBVS, 5670
Lacy, C. H. S. 2009, IBVS, 5910
Lacy, C. H. S. 2011, IBVS, 5972
Lacy, C. H. S. 2014, IBVS, 6098
Lacy, C. H. S., & Fekel, F. C. 2011, AJ, 142, 185
Lacy, C. H. S., Torres, G., & Claret, A. 2008, AJ, 135, 1757
Latham, D. W. 1992, in IAU Coll. 135, Complementary Approaches to Double and Multiple Star Research, ASP Conf. Ser. 32, ed. H. A. McAlister & W. I. Hartkopf (San Francisco, CA: ASP), 110
Latham, D. W., Nordström, B., Andersen, J., et al. 1996, A&A, 314, 864
Latham, D. W., Stefanik, R. P., Torres, G., et al. 2002, AJ, 124, 1144
Levi-Civita, T. 1937, AmJM, 59, 225
Lyubimkov, L. S., Rachkovskaya, T. M., & Rostopchink, S. I. 1996, ARep, 40, 802
Nordström, B., Latham, D. W., Morse, J. A., et al. 1994, A&A, 287, 338
North, P., & Debernardi, Y. 2004, in ASP Conf. Ser. 318, Spectroscopically and Spatially Resolving the Components of the Close Binary Stars, ed. R. W. Hilditch, H. Hensberge & K. Pavlovski (San Francisco, CA: ASP), 297
Pavlovski, K., & Hensberge, H. 2005, A&A, 439, 309
Pavlovski, K., Southworth, J., Kolbas, V., & Smalley, B. 2014, MNRAS, 438, 590
Popper, D. M. 1980, ARA&A, 18, 115
Popper, D. M., & Etzel, P. B. 1981, AJ, 86, 102
Preston, G. W. 1974, ARA&A, 12, 257
Prieur, J.-L., Carquillat, J.-M., & Imbert, J. 2006, MNRAS, 372, 703
Ramírez, I., Fish, J. R., Lambert, D. d L., & Allende Prieto, C. 2012, ApJ, 756, 46
Scarfe, C. D. 2010, Obs, 130, 214
Sebastian, D., Guenther, E. W., Schaffenroth, V., et al. 2012, A&A, 541, A34
Simon, K. P., & Sturm, E. 1994, A&A, 281, 286
Smalley, B., Smith, K. C., & Dworetsky, M. M. 2001, UCLSYN User Guide, available at http://www.astro.keele.ac.uk/~bs/publs/uclsyn.pdf
Southworth, J. 2011, MNRAS, 417, 2166
Tamajo, E., Pavlovski, K., & Southworth, J. 2011, A&A, 526, A76
Torres, G. 2010, AJ, 140, 1158
Torres, G., Andersen, J., & Giménez, A. 2010, A&ARv, 18, 67
Torres, G., Clausen, J. V., Bruntt, H., et al. 2012, A&A, 537, A117
Torres, G., Neuhäuser, R., & Guenther, E. W. 2002, AJ, 123, 1701
Torres, G., Stefanik, R. P., Andersen, J., et al. 1997, AJ, 114, 2764
Wachmann, A. A. 1966, AAHam, 7, 341
Yi, S., Demarque, P., Kin, Y.-C., et al. 2001, ApJS, 136, 417
Zejda, M., Mikulasek, Z., & Wolf, M. 2006, IBVS, 5741
Zucker, S., & Mazeh, T. 1994, ApJ, 420, 806